Hydrodynamics and local mass transfer characterization under gas–liquid–liquid slug flow in a rectangular microchannel

Liu, Yanyan; Yue, Jun; Xu, Chao; Zhao, Shuainan; Yao, Chaoqun; Chen, Guangwen

Published in:
AIChE Journal

DOI:
10.1002/aic.16805

Hydrodynamics and local mass transfer characterization under gas-liquid-liquid slug flow in a rectangular microchannel

Dedicated to the 70th anniversary of Dalian Institute of Chemical Physics, CAS

Yanyan Liu[1,2,3], Jun Yue[2], Chao Xu[1], Shuainan Zhao[1], Chaoqun Yao[1*] and Guangwen Chen[1*]

1. Dalian National Laboratory for Clean Energy, Dalian Institute of Chemical Physics, Chinese Academy of Sciences, Dalian 116023, China

2. Department of Chemical Engineering, Engineering and Technology Institute Groningen, University of Groningen, 9747 AG Groningen, The Netherlands

3. University of Chinese Academy of Sciences, Beijing 100049, China

Abstract

Gas-liquid-liquid three-phase slug flow was generated in a glass microreactor with rectangular microchannel, where aqueous slugs were distinguished by relative positions to air bubbles and organic droplets. Oxygen from bubbles reacted with resazurin in slugs, leading to prominent color changes, which was used to quantify mass transfer performance. The development of slug length indicated a film flow through the corner between bubbles and the channel wall, where the aqueous phase was saturated with oxygen transferred from bubble body. This film flow results in the highest equivalent oxygen concentration within the slug led by a bubble and followed by a droplet. The three-phase slug flow sub-regime with alternate bubble and droplet was found to benefit the overall mass transfer performance most. These results provide insights into a precise

[*] Corresponding author. Tel.: +86-411-8437-9031, Fax.: +86-411-8469-1570

E-mail address: gwchen@dicp.ac.cn (G.W. Chen), superyao@dicp.ac.cn (C.Q. Yao)

manipulation of gas-liquid-liquid slug flow in microreactors and the relevant mass transfer behavior thereof.

Keywords: mass transfer, multiphase flow, slug flow, microreactor, colorimetric method

Introduction

In the past few decades, the application of microreactors for process intensification has drawn much attention from both the academic and industrial communities[1-3]. With the lateral dimension of the inherent channel decreased to below ca. 1 mm, microreactors provide a much short diffusion distance and large interfacial area in multiphase systems. These characteristics lead to mass transfer coefficients therein being at least 1-2 orders of magnitude higher than those in conventional reactors[4,5]. A precise control over multiphase flow (*e.g.*, uniform bubbly, slug and parallel flows) and significantly reduced back-mixing are easily achieved in microreactors. These merits make microreactors not only a promising tool to measure physical and chemical properties (*e.g.*, diffusion coefficient[6,7] and kinetic parameters[8]), but also an piece of efficient equipment for carrying out various (chemical) processes where the system performance can be precisely elucidated[9-11]. Other benefits such as simplicity in scaling up and enhanced safety[12], further increase the economic and technical potentials of implementing microreactors in industries. Hence, microreactors have been widely employed in biomedical science[13], chemistry and chemical engineering[1-3,12,14,15].

Gas-liquid-liquid three-phase systems in microreactors have recently received more and more research attention, due to their great application potential, particularly in the intensification of extraction and reactions therein[16,17]. For example, as an inert gas was introduced to liquid-liquid extraction systems, the mass transfer coefficient could be

enhanced by around two folds[18-20] or up to two orders of magnitude[21], compared to its counterparts without gas agitation. Besides, gas-liquid-liquid flow in microreactors could benefit three-phase reaction systems, such as chemical synthesis under aqueous-organic catalysis (e.g., hydrogenation)[8,22]. Among the above processes, gas-liquid-liquid slug flow is the most commonly employed flow regime[23,24], due to its wide operating range and finer degree of controllability compared to others (*e.g.*, parallel flow and double emulsion system[11]). However, complex mass transfer scenarios[25-27] are usually involved, as shown in Fig. 1. If the reaction is assumed to occur in the continuous phase, gas (*e.g.*, H_2) has to be transferred to the continuous phase, where it is consumed and converted to a target product. In the case of reaction-extraction coupling process[25] (Fig. 1a), the target product formed in the continuous phase is further extracted into the dispersed droplet. In the case of a three-phase reaction, the mass transfer of liquid reactants from the dispersed phase to the continuous phase (or at least towards the interface at which the reaction takes place) is involved, as shown in Fig. 1b. Alternatively, the reaction could also occur in the droplet phase (Fig. 1c), where consecutive mass transfer steps (*e.g.*, gas transferring through the continuous phase to the dispersed phase) are involved. These multi-step mass transfer processes are much likely to limit the overall extraction/reaction performance if done in conventional reactors. Therefore, microreactors with their inherently high mass transfer efficiency are expected to be a promising tool for the intensification of these processes.

Figure 1. Schematics of mass transfer in a gas-liquid-liquid three-phase system in the microreactor. A, B are the reactants and P the product. The subscripts 1 and 2 represent

the continuous phase and the dispersed phase, respectively. Catalyst and reaction both reside in either of the continuous phase and the dispersed droplet phase.

The gas-liquid-liquid three-phase system in microreactors has shown an excellent performance in the processes mentioned above, due to the enhanced heat/mass transfer rate resulting from the intensified internal circulation and enlarged interfacial area. Zhang et al.[28] introduced an inert gas phase to the highly exothermic Beckmann rearrangement of cyclohexanone in oleum in a microreactor. Their study demonstrated that the gas bubble between droplets largely prevented coalescence and provided more evaporation space for heat removal, leading to a remarkably improved reaction rate and selectivity. As an example of three-phase chemical synthesis, Önal et al.[8] investigated the selective hydrogenation of α, β-unsaturated aldehydes with an aqueous catalyst (*i.e.*, Ru(II)-TPPTS) in a microreactor under gas-liquid-liquid slug flow. Their results showed that uniformly dispersed gas bubbles and aqueous droplets within this regime enabled an accurate mediation of the interfacial area for increased mass transfer, which is crucial for the kinetic study. Under the same flow regime, Yap et al.[22,26] showed that the hydrogenations of several olefins (*e.g.*, hexane, styrene and nitrobenzene) with Rh nanoparticle catalysts loaded in the dispersed aqueous phase achieved higher conversions and yields within a few minutes in a capillary microreactor, when compared with its batch counterpart. This is because of the significant acceleration of mass transfer rate caused by shorter diffusion distance in the microreactor. Yet, the overall performance was still limited by either the gas-liquid or liquid-liquid mass transfer during the reaction period even in their capillary microreactor[22,29].

From the above summary, one can conclude that precise control over mass transfer is crucial for optimizing the process performance in microreactors. Nevertheless, researches on mass transfer behavior in the gas-liquid-liquid microflow have so far been confined to the level of the global transfer coefficient characterization, rather than the local transfer mechanism elucidation. In most cases, the overall extraction/reaction performance with inert gas addition has been reported to increase under gas-liquid-liquid slug flow[18-21,28,30]. However, Assmann et al[20]. pointed out that the enhancement in mass transfer by gas addition only occurred at flow velocities above 0.08 m/s, while no notable difference presented at lower flow velocities. Ufer et al.[31] reported a significantly decreased mass transfer rate when the rear end of an aqueous droplet attached to an inert gas bubble, though the internal slug circulation was intensified. It emphasized the importance of the mass transfer between the rear end of the aqueous droplet and the continuous slug. Regarding systems with soluble or reacting gases, Yao et al.[32] showed that before the bubble and droplet contacted, the inert water droplet could intensify gas-to-oil mass transfer, whereas the mass transfer rate could be impeded after contacting. These results indicate that understanding the global mass transfer characteristics within a gas-liquid-liquid slug flow is not enough for the accurate manipulation of the corresponding process towards realizing the optimized performance in the microreactor. Further insights into local mass transfer details are needed, which require dedicated experimental characterization as well as numerical studies.

As a first step to unravel the complex mass transfer behavior within gas-liquid-liquid slug flow in microreactors (e.g., as illustrated in Fig. 1), this work has focused on the characterization of mass transfer from gas bubbles to the continuous phase

(i.e., in the presence of inert organic droplets)[24,33]. To obtain the local mass transfer information and avoid the end mass transfer effect associated with the offline sampling process[4,5,34], an online colorimetric method was employed based on the oxidation-reduction reaction of resazurin[35]. This method, previously applied successfully in gas-liquid slug flow in microreactors[35-37], has been extended to gas-liquid-liquid three-phase slug flow in this work. The gas-liquid-liquid slug flow was generated in a rectangular microchannel (fabricated on a glass plate) with double T-junctions. The aqueous solution (containing resazurin) was the continuous phase, air and 1-octanol as the dispersed phases. The color change in the aqueous slug length along the microreactor was monitored via flow visualization, followed by the analysis of the contribution of the film flow (which passed through the channel corner) to the overall mass transfer rate. Then, mass transfer performance in both gas-liquid-liquid and gas-liquid slug flows has been compared to better elucidate the effect of the inert organic phase. Favorable unit cell configurations within gas-liquid-liquid slug flow have been finally proposed in terms of the maximized mass transfer rate.

Materials and Methods

Colorimetric method and fluid properties

The involved reactions in the colorimetric method are shown in Fig. 2. Before being injected into the microchannel, the resazurin (sodium salt, Sigma Aldrich®, CAS 62758-13-8, molecular mass: 251.17 g/mol) solution in water was completely reduced to the colorless dihydroresorufin via pink resorufin, by glucose (Aladdin®, CAS 14431-43-7) and sodium hydroxide (Aladdin®, CAS 1310-73-2) under an oxygen-free

environment (N_2 flush). As the colorless dihydroresorufin contacted oxygen (in air bubbles) in the microchannel, dihydroresorufin would be instantly oxidized back to pink resorufin whose gray value was then used to quantify the amount of transferred oxygen. This reaction system provides a high contrast associated with color change for a given concentration variation[35-37] and thus enables an accurate concentration estimation. Furthermore, the large molecular size of dihydroresorufin/resorufin limits its diffusion into the film region near the gas-liquid interface (i.e., the main reaction in the liquid bulk)[7]. As a result, an enhancement factor very close to 1 is obtained, based on which direct measurement of the physical mass transfer coefficients is possible[7].

Figure 2. Reactions involved in the colorimetric method used for mass transfer characterization (reproduced from Ref[7]).

Based on the literature[7,35,36] and our preliminary experiments, 0.3 g/L resazurin solution with 20 g/L glucose and 20 g/L sodium hydroxide served as the aqueous phase in this work. At such concentration levels, the oxygen content in the gas phase (air) was always in a large excess under the operating conditions involved (*i.e.*, at least 10 times higher than needed for the reaction). To avoid the effect of the unexpected side reactions (i.e., the deprotonation and subsequent oxidation of glucose)[38,39] on the fluid properties (*e.g.*, gray level and viscosity), the aqueous feed solution was freshly made in each run and used only for maximum 40 minutes. Within this time interval, the surface tension and viscosity of the aqueous solution were constantly monitored and found to be stable at 73 mN/m (measured by DataPhysics OCA 15EC, Germany) and 1.29 mPa s (measured by a

viscometer DV-II+Pro, Brookfield, USA). Air and *n*-octane (Aladdin®, CAS 111-65-9) served respectively as the gas phase and the inert organic phase in the microreactor (vide infra). A summary of the fluid properties is given in Table 1.

Table 1. Physical properties of the used working fluids (20 ^{o}C, 0.1 Mpa)

Experimental Setup and Procedure

The glass-based microreactor with double T-junctions is sketched in Fig. 3. The meandering microchannel after the second T-junction (denoted as T2) is composed of straight channel segments that are mostly 20 mm long (except for the first and the last ones being 12 mm long) and jointed by half circles (radius r_c=1 mm), resulting in a total length of 440 mm. All channels are of 600 μm in width and 300 μm in depth (*i.e., w=600* μm, *h*=300 μm). In the experiments, both *n*-octane and the aqueous solution with resazurin were flushed by N_2 first and then respectively injected through inlets 1 and 2 to the first T-junction (denoted as T1) by syringe pumps (LSP02-1B, LongerPump, China). The liquid-liquid two-phase flow formed at T1 was stabilized in the microchannel between two T-junctions (about 110 mm long). Air was delivered from a pressurized gas bottle to inlet 3 through a pre-calibrated mass flow meter (SC200, Sevenstar, China), followed by a segment of the very thin capillary (inner diameter 20 μm, length 50 mm) to stabilize the gas flow. Thereafter, the gas-aqueous-organic three-phase slug flow was generated at the second T-junction. The flow regime and color change within the aqueous phase in the microchannel were recorded by a high-speed CMOS camera (Phantom M310, Vision Research, USA, working at 100-500 frames/s) with the aid of an optical

microscope (SZX 16, Olympus, USA). The microreactor was illuminated by a metal halide light source (MME-250, MORITEX SCHOTT). The viewing section under low magnification (×0.8) was shown by the blue dotted box in Fig. 3, and the recorded images (800×1280 pixels) resulted in a resolution of ca. 0.0176 mm/pixel, showing the overall flow regime. A higher magnification (×2.0; ca. 0.0071 mm/pixel) was employed to improve the accuracy of post-treatment in mass transfer analysis, with the observation area shown by the red solid box in Fig. 3. The volumetric flow ranges for the gas, aqueous and organic phases were 0.207-0.995, 0.30-1.00 and 0.10-1.00 mL/min, respectively. All experiments were conducted at room temperature (20±2 ^{o}C) and ambient pressure (0.1 MPa).

Figure 3. Structure of the microreactor (horizontally placed) used in three-phase flow and mass transfer study. The viewing sections for flow visualization and mass transfer characterization are indicated by the blue dotted box and the red solid box, respectively.

To better illustrate the effect of the organic phase addition on mass transfer performance, gas-aqueous two-phase flow as a benchmark was conducted. Here, the total aqueous flow was evenly injected to inlets 1 and 2 to reduce the flow fluctuation. The other experimental details were unchanged. For simplicity, the flow rate conditions in one experimental run are expressed using the notation as gas flow rate (Q_G)-aqueous flow rate (Q_W)-organic flow rate (Q_O) with units being mL/min. For example, the condition ‘G0.1-W0.6-O0.2’ refers to the gas, aqueous and organic flow rates being 0.1, 0.6 and 0.2 mL/min, respectively. A similar notation was used for gas-aqueous two-phase flow,

without the third term for the organic phase.

Image Processing

The relationship between the gray difference (ΔG) and the equivalent oxygen molar concentration (C; equal to half of the initial molar concentration of resazurin in the aqueous solution at a full resazurin conversion) was calibrated by the following procedure:

- preparing the calibration solutions with different resazurin concentration levels, namely, at 0 (blank solution as the reference), 0.042, 0.099, 0.139, 0.198, 0.258 and 0.305 g/L (corresponding to C = 0, 0.083, 0.196, 0.277, 0.394, 0.513 and 0.589 mol/m^3);
- the calibration solutions were well stirred under air, to ensure that resazurin therein was completely converted into the pink resorufin, and then injected to the microchannel immediately.
- the calibration images were first taken near the outlet of the microreactor to ensure the full conversion of resazurin under gas-liquid slug flow (Fig. 4a);
- then the calibration was proceeded using the image of the blank solution flowing in the microchannel as the background image. The gray difference for each calibration image was calculated by subtracting the corresponding gray level from the background image, and then correlated with the oxygen concentration as shown in Fig. 4b. As can be seen, the ΔG-C calibration curve turned out to be a quadratic instead of a linear relationship, perhaps due to the difference in the employed light sources (*i.e.*, a point light source in this work and a surface light

source LitePad HO LED backlight in the referred literature)[35-37]. The point light source also caused a gray distribution along the channel length. To minimize the processing uncertainties, only the middle part of the image ranging from 280 to 1080 pixels (see Fig. S1) were analyzed, ensuring the overall error below 10% (Fig. S2).

Figure 4. (a). Background and calibration images for the aqueous phase under various resazurin concentrations near the microreactor outlet; (b). Calibration curve between the equivalent oxygen concentration and the gray difference.

For gas-aqueous-organic three-phase slug flow, the original image (Fig. 5a), captured from the red view box indicated in Fig. 3, was first converted to the gray image (Fig. 5b) by *Matlab* (Mathworks, R2017a). Then, bubble boundaries were determined according to the absolute gray values in pixels during converting the gray image into the binary image, as shown in Fig. 5c. However, the same method is not practical for the droplet detection because: (1) the droplet border is much thinner and vaguer due to the small refraction index difference between the aqueous and organic phases; (2) the colorimetric reaction (*i.e.,* the color pink) within aqueous slugs lowered the gray value therein to be close to that of the droplet border, making it more difficult to distinguish the droplet border from the slug bulk. Therefore, a new approach based on the relative gray values was used to determine the droplet end caps, where only pixels with gray values smaller than their left neighbors (either in the droplet or the slug) by at least 10 gray units were marked as the droplet border. With this approach, only semicircular droplet caps

were obtained (Fig. 5d), while the borders of the droplet body (i.e., the more or less cylindrical part) that are parallel to channel wall could not be identified. Thus, the complete droplet zone (Fig. 5e) was further settled by combining a cap with its closest cap with the opposite orientation or an edge of the image. After combining the detected bubbles and droplets in one image (Fig. 5f), the gray difference in the slug was derived by subtracting the background from the gray image (Fig. 5b), resulting in a modified image as shown in Fig. 5g. Thereafter, the gray difference was converted to the normalized equivalent oxygen molar concentration (ranging from 0 to 1, denoted as $C_{norm} = C/C_{max}$, where C_{max}=0.589 mol/m^3 for the aqueous solution with 0.3 g/L resazurin) according to the calibration curve (Fig. 4b). Applying a jet colormap format, the C_{norm} distribution within the aqueous slug was finally visualized in the calibrated image (Fig. 5h), where bubbles and droplets were respectively marked by black and dark blue (corresponding to C_{norm} = 0 in droplets). The identification of bubbles and slugs for gas-aqueous two-phase systems did not involve steps shown in Figs. 5(d-f).

Figure 5. Identification process of bubbles and droplets in gas-aqueous-organic slug flow (G0.2-W0.6-O0.4, the gas, aqueous and organic phases are respectively air, 0.3 g/L resazurin solution with 20 g/L glucose and 20 g/L sodium hydroxide, and *n*-octane) in the microreactor: (a). original image; (b). gray image; (c) bubbles, (d) droplet caps, (e) droplets and (f) bubbles and droplets detected in binary images; (g) modified image after subtracting the background; (h) calibrated image with the normalized equivalent oxygen molar concentration (ranging from 0 to 1).

Results and Discussion

This section presents the details on hydrodynamics and mass transfer characterization under a gas-liquid-liquid three-phase slug flow in the rectangular microreactor.

Hydrodynamics

In this work, gas-liquid-liquid slug flow was generated by penetrating gas tip into liquid-liquid slug flow at T2 (Fig. 3). Due to the rigid gas-liquid interface, the rupture of gas tip depended on the exact phase it contacted (*i.e.*, bubbles were either squeezed by the aqueous phase or cut by the organic droplet body/cap)[32], which presented a periodic behavior related to the droplet/slug lengths within the aqueous-organic slug flow generated at T1 and the gas flow rate at T2. During experiments, three typical sub-regimes were identified according to the number and relative position of droplets and bubbles within a unit cell (UC), as shown in Figs. 6a and 6b:

- One preceding organic droplet followed by two bubbles (B2D1), which occurred at relatively high gas-organic flow ratios under the current conditions (more specifically $Q_G/Q_W > 0.64Q_O/Q_W + 0.10$; cf. Fig. 6b). In this case, two bubbles were generated in a unit cell due to the squeezing and cutting by the aqueous phase at T2. Three organic slug types are involved here: (1) slug BSD, which locates between a preceding droplet and a following bubble (1st bubble); (2) slug BSB, between two bubbles (1st and 2nd bubbles) and (3) slug DSB, between a preceding bubble (2nd bubble) and a droplet in the next unit cell.
- One preceding organic droplet followed by one bubble (B1D1), which emerged at intermediate gas-organic flow ratios ($0.18Q_O/Q_W + 0.10 < Q_G/Q_W <$

$0.64Q_O/Q_W + 0.10$). This sub-regime, where both slugs BSD and DSB were involved, was most commonly reported in the literature[11,32].

- Two sequential organic droplets followed by one bubble (B1D2), which presented under relative low gas-organic flow ratios ($Q_G/Q_W < 0.18Q_O/Q_W + 0.10$). Despite slugs BSD and DSB, a new slug type DSD residing between the 1st and 2nd droplet was generated.

Figure 6. (a). Typical sub-regimes and slug types observed during experiments; (b). Sub-regime map of gas-liquid-liquid slug flow in the current microreactor.

A distinguishing characteristic of gas-liquid-liquid slug flow with low viscosity fluids in rectangular microchannels is that gas bubbles move faster than droplets[24,32]. It is well known that for two-phase slug flow in circular microchannels, the bubble/droplet velocity is positively related to the film thickness between the bubble/droplet body and the microchannel wall, and further to the capillary number *Ca*[40-42]. Accordingly, the bubble velocity should be smaller than that of the organic droplet in the gas-liquid-liquid slug flow therein[43], since *Ca* for the bubble is smaller than that for the organic droplet due to the interfacial tension difference. However, the opposite phenomenon was observed in our experiments, which is caused by 1) the larger density contrast between gas bubbles and the aqueous phase, which leads to near stagnant film around bubbles, while the aqueous film around the organic droplet is moving at a velocity more or less equal to the droplet[44]. 2) the rectangular microchannel used in our work opened a large corner area between the bubble body and channel wall. To show the relative motion of

bubbles and droplets more clearly, Fig. 7 presents the evolution of slug lengths versus the dimensionless residence time τ_{norm}. Note that τ_{norm} is normalized by the time interval that the slug flow needs to pass the length of a unit cell (L_{UC}), while the dimensional residence time $\tau = L_{ch}wh/(Q_W+Q_O+Q_G)$ (L_{ch} is the distance between T2 and the concentration measurement location) in the sub-regime B2D1 (see Eq. S4). As shown in Fig. 7a, the length of a unit cell (L_{UC}) remained constant with the increase of τ_{norm}, whereas both the length of the slug DSB (L_{DSB}) increased and that of the slug BSD (L_{BSD}) decreased linearly. These length variations indicate the presence of a liquid film flow (taking the bubble as the reference frame) through the corner gap, eventually leading to the collision of the first bubble and the leading droplet, as shown in Fig. 7b (τ_{norm} = 9.22). The length of the slug BSB (L_{BSB}) remained unchanged until the collision started, due to the equal velocities between the preceding and trailing bubbles. After the collision, the velocity of the formed bubble-droplet cluster decreased (76.8 mm/s in Fig. 7b), which was slightly lower than the original bubble velocity (77.3 mm/s), but still higher than the droplet velocity (74.6 mm/s). Accordingly, L_{BSB} began to decrease and the increase rate of L_{DSB} slowed down. Eventually, the flow would reach stable with only bubble-droplet clusters, which are expected to hinder the mass transfer if the solubility of the gas in droplets is smaller than that in the continuous phase[32], but to intensify the mass transfer in the opposite case[45].

Figure 7. (a). Change of slug lengths with the dimensionless residence time and (b) the corresponding images within a unit cell under the sub-regime B2D1 in the microreactor. Operating condition: G0.2-W0.6-O0.1.

Mass Transfer

It was observed that the mass transfer rates varied significantly in the current rectangular microreactor, according to different slug types in gas-liquid-liquid flow. Fig. 8 presents these normalized oxygen concentrations C_{norm} in the aqueous slugs. Taking the sub-regime B2D1 (Figs. 8a-b) as an example, C_{norm} values in the slug DSB were much higher than those in slugs BSB and BSD. There are two possible reasons for this phenomenon: 1) more significant internal circulation in the shorter slug DSB compared with the slug BSB; 2) the mixing of the slug with film flow (where C and C_{norm} were relatively high) as the bubble passed by. The second contribution dominated since similar results were also found under the sub-regime B1D1 as shown in Fig. 8c, where the length of slug DSB equals to (*i.e.*, at τ_{norm} = 0) or even longer (*i.e.*, at τ_{norm} = 3.44, 5.97 and 10.49) than that of the slug BSD. This is in line with the literature results that the film flow made a significant contribution to mass transfer in two-phase slug flow[46].

Figure 8. Normalized equivalent oxygen molar concentration (C_{norm}) in aqueous slugs under gas-liquid-liquid flow in the microreactor. (a) C_{norm} distribution and (b) the development of C_{norm} with the dimensionless residence time τ_{norm} along the microchannel under the sub-regime B2D1; operating condition: G0.2-W0.6-O0.1; (c) C_{norm} distribution within slugs DSB and BSD that have equal initial lengths under the sub-regime B1D1 at different τ_{norm} values; operating condition: G0.2-W0.6-O0.2.

The effect of the film flow on mass transfer under gas-liquid-liquid three-phase slug

flow in the rectangular microreactor is quantitatively analyzed as the following. The sub-regime B1D1 was chosen in this case for its simplicity, and the mass transfer scenario in the film region is depicted in Fig. 9. In a reference frame with the wall moving at the bubble speed, the liquid film moves backward from the bubble front to the rear. It is assumed that the film flow reaches a perfect mixing with the slug bulk immediately after contact. As mentioned above, there's no aqueous film flow around organic droplets, nor free oxygen molecule in organic droplets, the contribution of film flow around droplets was hence negligible. Therefore, the mass transfer of oxygen in aqueous slugs arouse from either the bubble cap or the film flow. Accordingly, the mass balance of oxygen in slugs DSB and BSD respectively follow

$$\frac{dn_{DSB}}{d\tau} = k_{L,cap} A_{cap} C^* + Q_{film} C_{film,out} \tag{1}$$

$$\frac{dn_{BSD}}{d\tau} = k_{L,cap} A_{cap} C^* - Q_{film} C_{film,in} \tag{2}$$

where n_{DSB} and n_{BSD} are the amounts of the equivalent oxygen (in mol) within slugs DSB and BSD in a single unit cell, respectively. Q_{film} is the volumetric flow rate of the liquid film in the reference frame, $C_{\mathrm{film,in}}$ and $C_{\mathrm{film,out}}$ are the equivalent oxygen concentrations in the liquid film at the film inlet and outlet, respectively. According to the perfect-mixing assumption, $C_{\mathrm{film,in}}$ equals to C_{BSD}. The mass balance within the liquid film gives

$$Q_{film}\left(C_{film,out} - C_{film,in}\right) = k_{L,film} A_{film} C^* \tag{3}$$

Rearranging Eq. (3) leads to

$$C_{film,out} = \frac{k_{L,film} A_{film}}{Q_{film}} C^* + C_{film,in} \tag{4}$$

With Eqs. (1), (2) and (4), the ratio between the amount of equivalent oxygen

transferred from the film-slug mixing and that from the bubble cap can be described by $C_{\mathrm{film,out}}Q_{\mathrm{film}}/k_{\mathrm{L,cap}}A_{\mathrm{cap}}C^{*}$ in the slug DSB, and $C_{\mathrm{film,in}}Q_{\mathrm{film}}/k_{\mathrm{L,cap}}A_{\mathrm{cap}}C^{*}$ in the slug BSD. The transient ratio of the accumulation rate of the equivalent oxygen within the slug DSB to that within the slug BSD in the current microchannel could be simply estimated by

$$\frac{dn_{DSB}}{d\tau}\Big/\frac{dn_{BSD}}{d\tau}=\left(1+\frac{Q_{film}C_{film,out}}{k_{L,cap}A_{cap}C^{*}}\right)\Big/\left(1-\frac{Q_{film}C_{film,in}}{k_{L,cap}A_{cap}C^{*}}\right) \tag{5}$$

Note that the mass transfer coefficients (i.e., $k_{\mathrm{L,cap}}$ and $k_{\mathrm{L,film}}$) in Eqs. (3-5) were estimated by treating the current rectangular microchannel as a round capillary with the same hydraulic diameter[40,47], and the interface areas of bubble cap and film (A_{cap} and A_{film}) were calculated according to the bubble shape proposed by Musterd et al[48]. The film flow rate Q_{film} was extracted from the recorded images (×2.0 magnification), by multiplying the increasing rate of L_{DSB} (or shortening rate of L_{BSD}, cf. Fig. 7a before the collision occurred) with the cross-sectional area of the microchannel (see Eqs. (S6-16) for details).

Figure 9. Sketch of mass transfer in the liquid film within a unit cell under the sub-regime B1D1, depicted in a half channel (microchannel corner being exaggerated).

Table 2 summarizes the calculation results based on the analysis above, taking G0.2-W0.6-O0.3 as an example. It can be seen that in a slug DSB, the amount of equivalent oxygen transferred from the film flow was several times higher than that from the bubble cap (i.e., $C_{\mathrm{film,out}}Q_{\mathrm{film}}/k_{\mathrm{L,cap}}A_{\mathrm{cap}}C^{*}$ = 5-6), and these values did not vary much with the increase of $C_{\mathrm{film,in}}$ (= C_{BSD}). From Eq. (4), we can see that $C_{\mathrm{film,out}}$ is composed of two parts: one is due to the contact between the liquid film and bubble body, and the other from the perfectly mixed slug BSD. The stable $C_{\mathrm{film,out}}Q_{\mathrm{film}}/k_{\mathrm{L,cap}}A_{\mathrm{cap}}C^{*}$ values

indicates that $C_{film,out}$ is dominated by the first part. The transient ratio of the equivalent oxygen accumulation $(dn_{DSB}/d\tau)/(dn_{BSD}/d\tau)$ increases with the dimensionless residence time τ_{norm}, and is always larger than 6. Fig. 10 shows the measured amount of the equivalent oxygen accumulated in slugs DSB and BSD (n_{DSB} and n_{BSD}), which were obtained experimentally by adding up the product of the equivalent oxygen concentration and the channel volume in each pixel. The measured ratios n_{DSB}/n_{BSD} (determined from Fig. 10 as 3.61, 4.91 and 6.14 for τ_{norm} = 3.98, 6.49 and 10.50, respectively) also increase with τ_{norm}, but the absolute values are much smaller than the transient ones (> 6) as listed in Table 2. Despite that the measured n_{DSB}/n_{BSD} values are equal to the definite integral of the transient ratio over the residence time interval [0, τ], the discrepancy still cannot be justified. This discrepancy is caused by the saturation of liquid film that was not considered in the calculation, e.g., the calculated $C_{film,out}$ by Eq. (4) equals to at least 1.749 mol/m^3 (as τ_{norm} = 0 and C_{BSD} = 0 mol/m^3) while C_{max} = 0.589 mol/m^3 for the applied aqueous phase (i.e., 0.3 mol/m^3 resazurin). After adjusting values of $C_{film,out}$ to C_{max}, new transient ratios calculated with Eq. (5) become 3.36, 4.01 and 5.30 for τ_{norm} = 3.98, 6.49 and 10.50, respectively, which would lead to smaller n_{DSB}/n_{BSD} predictions compared with the experimental results. This underestimation of n_{DSB}/n_{BSD} is possibly because of the imperfect mixing inside the slug BSD. The local equivalent oxygen concentration at the bubble cap side was much larger than that at the droplet cap side, as only the former transfers oxygen to the liquid phase. In other words, the actual value of $C_{film,in}$ used in Eq. (5) should be larger than C_{BSD} as an averaged value, leading to a larger $(dn_{DSB}/d\tau)/(dn_{BSD}/d\tau)$.

Table 2. Mass transfer contribution of the film flow in rectangular microchannel under sub-regime B1D1 with the perfect film-slug mixing assumption[*].

[*]Under operating conditions G0.2-W0.6-O0.3, the relating parameters were $k_{L,cap}$=1.55×10^{-3} m/s, $k_{L,film}$=1.27×10^{-3} m/s, A_{film}=1.62×10^{-6} m^2 and Q_{film}=0.018 mL/min.

Figure 10. Accumulation of the amount of the equivalent oxygen in slugs BSD and DSB under the sub-regime B1D1 with operating conditions shown in the figure.

Comparison of Mass Transfer in Two-phase and Three-phase Systems

Fig. 11 shows the comparison of mass transfer performance between gas-liquid and gas-liquid-liquid slug flows at a given location of L_{ch}=27 mm in the microreactor, with a gas flow rate being 0.2 mL/min. For this comparison, the Reynolds number of the aqueous phase *Re* (see Eq. S5) was used to clarify the effect of the total flow rate on mass transfer. It can be seen from Fig. 11a that the specific interfacial area of bubbles (i.e., the ratio between the interfacial area of a bubble and the volume of the unit cell, determined from the recorded images as described in Eqs. (S6-11)) in two-phase flow decreased with the increase of *Re* values, in accordance with the literature[37]. The specific interfacial area in three-phase flow follows the same trend. Moreover, the variation of the interfacial area in two-phase and three-phase systems under the same *Re* was within 15%. This small difference is because that the gas phase fraction applied in these experiments was too small for the gas bubbles to be squeezed off by organic droplets[32] and generate more bubbles.

Fig. 11b displays that the normalized oxygen concentration C_{norm} in a unit cell for

two-phase flow decreases with the increase of *Re* (i.e., Q_W), due to the shortening of the residence time and larger slug volume in the unit cell. However, for gas-liquid-liquid systems with a fixed Q_W and Q_G, C_{norm} increased first and then decreased with the increase of *Re* (i.e., with increasing Q_O), indicating that the residence time is not the only influential factor. It was found that the increase in C_{norm} mainly happened during the sub-regime changing from B2D1 to B1D1, while the decrease in C_{norm} happened from B1D1 to B1D2. Apparently, the presence of too many droplets in the system (B1D2) is adverse to mass transfer compared with B1D1, as part of the aqueous phase in the unit cell (i.e., the slug DSD) was isolated from bubbles. As to the shift from B2D1 to B1D1, the increase in the mass transfer was expected due to both the intensified internal circulation and film-slug exchange, though the residence time is shortened.

Figure 11. Effect of *Re* on (a) the specific interfacial area of bubbles, and (b) the equivalent oxygen concentration under gas-aqueous and gas-aqueous-organic slug flows in the microreactor at a location of L_{ch} = 27 mm. In these figures, *Re* is directly related to the total liquid flow rate (i.e., Q_W+Q_O in the three-phase system and Q_W in the two-phase system).

Under a fixed residence time (*i.e.*, an identical *Re*), C_{norm} in the three-phase flow was found to be higher than that in two-phase flow (Fig. 11b), because Q_W in three-phase flow is actually smaller than that in gas-liquid two-phase flow. To further clarify the effect of the sub-regimes and the gas phase flow rate Q_G, the normalized oxygen concentrations within unit cells were compared under fixed aqueous and oil flow rates, as displayed in

Fig. 12. Clearly, C_{norm} in the three-phase flow was always larger than in two-phase flow. This agrees with our previous finding that the inert droplets (before the collision) serve as an agitator to intensify the gas-liquid mass transfer[30]. Under gas-liquid-liquid three-phase systems, the normalized oxygen concentration increased with the increase of the gas flow rate for a certain operating condition (e.g., Q_G-W0.8-O0.3), which is reasonable since the gas source and interfacial area were hence increased. More importantly, Fig. 12 again shows that mass transfer in the sub-regime B1D1 (for hydrodynamic characterization, see Fig. S5) is better than the other sub-regimes (e.g., B1D2 at low Q_G and B2D1 at higher Q_G) under a given gas flow rate. For example, at Q_G = 0.8 mL/min, the sub-regime B1D1 under the condition of 'Q_G-W0.8-O0.8' gave higher C_{norm} than the B2D1 sub-regime with 'Q_G-W0.8-O0.3', though the residence time in the former case is actually shorter than the latter.

Figure 12. Effect of the gas flow rate on the mass transfer performance in both gas-aqueous (open marks) and gas-aqueous-organic (solid marks) slug flow at the fixed location of L_{ch}=27 mm. The sub-regimes are indicated in the figure as well.

Conclusion

Gas-liquid-liquid microflow has gained more and more attention in both the academic and industrial communities, since these three-phase systems are frequently encountered in chemical syntheses (*e.g.*, hydrogenation). However, mass transfer mechanism therein has not been sufficiently studied yet, especially regarding the local mass transfer characterization and its relationship with hydrodynamics. This work

focused on the above aspects under gas-aqueous-organic three-phase slug flow using the visualization of resazurin-oxidation method.

Three sub-regimes were characterized according to the number of bubbles and droplets in a unit cell: (1) one preceding organic droplet followed by two bubbles (B2D1) (2) one preceding organic droplet followed by one bubble (B1D1) (3) two sequential organic droplets followed by one bubble (B1D2). These sub-regimes contained different types of aqueous slugs sandwiched by bubbles or droplets (e.g., slug types BSD, BSB, DSB and DSD; the slug BSD is sandwiched by a following bubble and a preceding droplet). The slugs DSB and BSD were respectively elongated and shortened along the channel, due to the faster movement of bubbles therein. This leads to a backward film flow (in the reference frame of bubbles) through the gap between the bubble body and channel wall, as well as an eventual bubble-droplet collision at a sufficiently long residence time.

More importantly, the film flow results in different mass transfer rates among slugs: that in the slug DSB is always the highest, while those in slugs BSB and BSD are respectively the medium and lowest, regardless of slug lengths. Through a semi-quantitative study under the sub-regime B1D1, the amount of oxygen transferred through the film flow was found to be several times of that from the bubble cap. Further study shows that the addition of an organic phase enhanced the mass transfer rate compared to the corresponding gas-liquid two-phase flow, and the sub-regime B1D1 benefits the best among all, which occurs as $0.18Q_O/Q_W + 0.10 < Q_G/Q_W < 0.64Q_O/Q_W + 0.10$. It implies the importance of precise control over the flow sub-regime for gas-liquid-liquid slug flow. This work is expected to improve the current understanding

into hydrodynamics and mass transfer, especially when it comes to the contribution of the liquid film under gas-aqueous-organic slug flow in a rectangular microchannel.

Notation

Roman symbols

A	m^2	Interfacial area or cross-sectional area
a	m^{-1}	Specific interfacial area of bubbles
C	mol/m^3	Equivalent oxygen concentration in a unit cell
C^*	mol/m^3	Saturated concentration of oxygen in the aqueous phase
h	m	Height of the microchannel
k_L	m/s	Liquid-side mass transfer coefficient
L	m	Length
n	mol	Amount of the equivalent oxygen transferred to the aqueous slug
Q	mL/min	Volumetric flow rate
Re	-	Reynolds number of the aqueous phase in a microflow
w	m	Width of the microchannel

Subscripts

BSB	Slug BSB
BSB	Slug BSB
cap	Bubble cap area
ch	microchannel

DSB	Slug DSB
film	Aqueous film around the bubble body
G	Gas phase
in	Inlet of the aqueous film
L	All liquid phases
max	Maximum value
norm	Normalized value
O	Organic phase
out	Outlet of the aqueous film
UC	Unit cell
W	Aqueous phase

Greek symbols

μ	mPa s	Viscosity
ρ	kg/m^3	Density of the aqueous solution
σ	mN/m	Interfacial tension
τ	s	Residence time along the microchannel

Acknowledgements

We gratefully acknowledge the financial support for this work from the National Natural Science Foundation of China (Nos. 21676263, 91634204 and U1608221) and the Youth Innovation Promotion Association CAS-China (No. 2017229). Yanyan Liu would like to acknowledge the China Scholarship Council for the financial support (No.

201704910487) of her study at the University of Groningen and Dr. Lixia Yang for the kind help on the preparation of resazurin solution.

Literature Cited

1. Jensen KF. Flow chemistry-Microreaction technology comes of age. *AIChE J.* 2017;63(3):858-869.
2. Jahnisch K, Hessel V, Lowe H, Baerns M. Chemistry in microstructured reactors. *Angew. Chem. Int. Ed. Engl.* 2004;43(4):406-446.
3. Mason BP, Price KE, Steinbacher JL, Bogdan AR, McQuade DT. Greener approaches to organic synthesis using microreactor technology. *Chem. Rev.* 2007;107(6):2300-2318.
4. Yue J, Chen GW, Yuan Q, Luo LA, Gonthier Y. Hydrodynamics and mass transfer characteristics in gas-liquid flow through a rectangular microchannel. *Chem. Eng. Sci.* 2007;62(7):2096-2108.
5. Zhao YC, Chen GW, Yuan Q. Liquid-liquid two-phase mass transfer in the T-junction microchannels. *AIChE J.* 2007;53(12):3042-3053.
6. Culbertson CT, Jacobson SC, Michael Ramsey J. Diffusion coefficient measurements in microfluidic devices. *Talanta.* 2002;56(2):365-373.
7. Yang LX, Dietrich N, Hébrard G, Loubière K, Gourdon C. Optical methods to investigate the enhancement factor of an oxygen-sensitive colorimetric reaction using microreactors. *AIChE J.* 2017;63(6):2272-2284.
8. Önal Ÿ, Lucas M, Claus P. Application of a Capillary Microreactor for Selective Hydrogenation of α,β-Unsaturated Aldehydes in Aqueous Multiphase Catalysis.

Chem. Eng. Technol. 2005;28(9):972-978.

9. Susanti, Winkelman JGM, Schuur B, Heeres HJ, Yue J. Lactic Acid Extraction and Mass Transfer Characteristics in Slug Flow Capillary Microreactors. *Ind. Eng. Chem. Res.* 2016;55(16):4691-4702.
10. Zhang Q, Liu H, Zhao SN, Yao CQ, Chen GW. Hydrodynamics and mass transfer characteristics of liquid–liquid slug flow in microchannels: The effects of temperature, fluid properties and channel size. *Chem. Eng. J.* 2019;358:794-805.
11. Yue J, Rebrov EV, Schouten JC. Gas-liquid-liquid three-phase flow pattern and pressure drop in a microfluidic chip: similarities with gas-liquid/liquid-liquid flows. *Lab chip.* 2014;14(9):1632-1649.
12. Zhang J, Wang K, Teixeira AR, Jensen KF, Luo G. Design and Scaling Up of Microchemical Systems: A Review. *Annu. Rev. Chem. Biomol. Eng.* 2017;8:285-305.
13. Shembekar N, Chaipan C, Utharala R, Merten CA. Droplet-based microfluidics in drug discovery, transcriptomics and high-throughput molecular genetics. *Lab chip.* 2016;16(8):1314-1331.
14. Wen ZH, Jiao FJ, Yang M, Zhao SN, Zhou F, Chen GW. Process Development and Scale-up of the Continuous Flow Nitration of Trifluoromethoxybenzene. *Org. Process Res. Dev.* 2017;21(11):1843-1850.
15. Tao S, Yang M, Chen HH, Ren MY, Chen GW. Microfluidic synthesis of Ag@Cu2O core-shell nanoparticles with enhanced photocatalytic activity. *J. Colloid Interface Sci.* 2017;486:16-26.
16. Chen Z, Xu JH, Wang YD. Gas-liquid-liquid multiphase flow in microfluidic systems - A review. *Chem. Eng. Sci.* 2019;202:1-14.

17. Schrimpf M, Esteban J, Rösler T, Vorholt AJ, Leitner W. Intensified Reactors for Gas-Liquid-Liquid Multiphase Catalysis: from Chemistry to Engineering. *Chem. Eng. J.* 2019.
18. Su YH, Chen GW, Zhao YC, Yuan Q. Intensification of liquid-liquid two-phase mass transfer by gas agitation in a microchannel. *AIChE J.* 2009;55(8):1948-1958.
19. Aoki N, Ando R, Mae K. Gas-liquid-liquid slug flow for improving liquid-liquid extraction in miniaturized channels. *Ind. Eng. Chem. Res.* 2011;50(8):4672-4677.
20. Assmann N, von Rohr PR. Extraction in microreactors: Intensification by adding an inert gas phase. *Chem. Eng. Process.: Process Intensification.* 2011;50(8):822-827.
21. Wang K, Qin K, Wang T, Luo GS. Ultra-thin liquid film extraction based on a gas-liquid-liquid double emulsion in a microchannel device. *RSC Adv.* 2015;5(9):6470-6474.
22. Yap SK, Yuan Y, Zheng L, Wong WK, Yan N, Khan SA. Rapid nanoparticle-catalyzed hydrogenations in triphasic millireactors with facile catalyst recovery. *Green Chem.* 2014;16(11):4654-4658.
23. Wang K, Lu YC, Qin K, Luo GS, Wang T. Generating Gas-Liquid-Liquid Three-Phase Microflows in a Cross-Junction Microchannel Device. *Chem. Eng. & Technol.* 2013;36(6):1047-1060.
24. Rajesh VM, Buwa VV. Experimental characterization of gas-liquid-liquid flows in T-junction microchannels. *Chem. Eng. J.* 2012;207-208:832-844.
25. Tan J, Dong C, Lu YC, Xu JH, Luo GS. Coupling process of oxidation and extraction in a gas-liquid-liquid microdispersion system for H_2O_2 synthesis. *Ind. Eng. Chem. Res.* 2012;51(4):1834-1845.

26. Yap SK, Yuan Y, Zheng L, Wong WK, Yan N, Khan SA. Triphasic segmented flow millireactors for rapid nanoparticle-catalyzed gas-liquid reactions-hydrodynamic studies and reactor modeling. *J. Flow Chem.* 2014;4(4):200-205.
27. Chaudhari RV, Bhattacharya A, Bhanage BM. Catalysis with soluble complexes in gas-liquid-liquid systems. *Catal. Today.* 1995;24(1-2):123-133.
28. Zhang JS, Wang K, Lin XY, Lu YC, Luo GS. Intensification of fast exothermic reaction by gas agitation in a microchemical system. *AIChE J.* 2014;60(7):2724-2730.
29. Karan D, Khan SA. Mesoscale triphasic flow reactors for metal catalyzed gas-liquid reactions. *React. Chem. Eng.* 2019.
30. Abolhasani M, Bruno NC, Jensen KF. Oscillatory three-phase flow reactor for studies of bi-phasic catalytic reactions. *Chem. Comm.* 2015;51(43):8916-8919.
31. Ufer A, Sudhoff D, Mescher A, Agar DW. Suspension catalysis in a liquid-liquid capillary microreactor. *Chem. Eng. J.* 2011;167(2-3):468-474.
32. Yao CQ, Liu Y, Zhao SN, Dong ZY, Chen GW. Bubble/droplet formation and mass transfer during gas-liquid-liquid segmented flow with soluble gas in a microchannel. *AIChE J.* 2017;63(5):1727-1739.
33. Liu Y, Yue J, Zhao SN, Yao CQ, Chen GW. Bubble splitting under gas-liquid-liquid three-phase flow in a double T-junction microchannel. *AIChE J.* 2018;64(1):376-388.
34. Li GX, Shang MJ, Song Y, Su YH. Characterization of liquid-liquid mass transfer performance in a capillary microreactor system. *AIChE J.* 2018;64(3):1106-1116.
35. Dietrich N, Loubière K, Jimenez M, Hébrard G, Gourdon C. A new direct technique for visualizing and measuring gas-liquid mass transfer around bubbles moving in a

straight millimetric square channel. *Chem. Eng. Sci.* 2013;100:172-182.

36. Yang LX, Dietrich N, Loubière K, Gourdon C, Hébrard G. Visualization and characterization of gas-liquid mass transfer around a Taylor bubble right after the formation stage in microreactors. *Chem. Eng. Sci.* 2016;143:364-368.
37. Yang LX, Loubière K, Dietrich N, Le Men C, Gourdon C, Hébrard G. Local investigations on the gas-liquid mass transfer around Taylor bubbles flowing in a meandering millimetric square channel. *Chem. Eng. Sci.* 2017;165:192-203.
38. Anderson L, Wittkopp SM, Painter CJ, et al. What Is Happening When the Blue Bottle Bleaches: An Investigation of the Methylene Blue-Catalyzed Air Oxidation of Glucose. *J. Chem. Educ.* 2012;89(11):1425-1431.
39. Oja SM, Guerrette JP, David MR, Zhang B. Fluorescence-enabled electrochemical microscopy with dihydroresorufin as a fluorogenic indicator. *Anal. Chem.* 2014;86(12):6040-6048.38. Aussillous P, Quéré D. Quick deposition of a fluid on the wall of a tube. *Phys. Fluids.* 2000;12(10):2367.
40. Aussillous P, Quéré D. Quick deposition of a fluid on the wall of a tube. *Phys. Fluids*. 2000;12(10):2367.
41. Yao CQ, Zhao YC, Ye CB, Dang MH, Dong ZY, Chen GW. Characteristics of slug flow with inertial effects in a rectangular microchannel. *Chem. Eng. Sci.* 2013;95:246-256.
42. Yao CQ, Zhao YC, Chen GW. Multiphase processes with ionic liquids in microreactors: hydrodynamics, mass transfer and applications. *Chem. Eng. Sci.* 2018;189:340-359.
43. Ładosz A, Rigger E, Rudolf von Rohr P. Pressure drop of three-phase

liquid-liquid-gas slug flow in round microchannels. *Microfluid Nanofluid.* 2016;20(3) 20:49.

44. Poesio P, Damone A, Matar OK. A multiscale approach to interpret and predict the apparent slip velocity at liquid-liquid interfaces. *J. Phys.: Conf. Ser.* 2017;923:012003.
45. Widianto AY, Aubin J, Xuereb C, Poux M. Gas-liquid-liquid reactions: Contacting mechanisms and effective process technologies. *Catal. Today*. 2019.
46. Vandu CO, Liu H, Krishna R. Mass transfer from Taylor bubbles rising in single capillaries. *Chem. Eng. Sci.* 2005;60(22):6430-6437.
47. Arsenjuk L, Kaske F, Franzke J, Agar DW. Experimental investigation of wall film renewal in liquid–liquid slug flow. *Int. J. Multiphase Flow.* 2016;85:177-185.
48. Musterd M, van Steijn V, Kleijn CR, Kreutzer MT. Calculating the volume of elongated bubbles and droplets in microchannels from a top view image. RSC Adv. 2015;5(21):16042-16049.

Table 1. Physical properties of the used working fluids (20 ^{o}C, 0.1 Mpa)

Phase	Fluid	Viscosity μ [mPa·s]	Density ρ [kg/m^3]	Surface tension σ [mN/m]
Organic	n-octane	0.565	702	21.14
Gas	air	0.0179	1.184	--
Aqueous	0.3 g/L resazurin with 20 g/L glucose/sodium hydroxide	1.29	1002	73

Table 2. Mass transfer contribution of the film flow in rectangular microchannel under sub-regime B1D1 with the perfect film-slug mixing assumption*.

τ_{norm} -	C_{BSD} mol/m^3	$C_{film,out}Q_{fil_m}/k_{L,cap}A_{cap}C^*$	$C_{film,in}Q_{fil_m}/k_{L,cap}A_{cap}C^*$	$\frac{dn_{DSB}}{d\tau}\Big/\frac{dn_{BSD}}{d\tau}$
0	0	5.43	0	6.43
3.98	0.05	5.59	0.16	7.85
6.49	0.09	5.73	0.30	9.61
10.50	0.15	5.90	0.47	13.02

*Under operating conditions G0.2-W0.6-O0.3, the relating parameters were $k_{L,cap}$=1.55×10^{-3} m/s, $k_{L,film}$=1.27×10^{-3} m/s, A_{film}=1.62×10^{-6} m^2 and Q_{film}=0.018 mL/min.

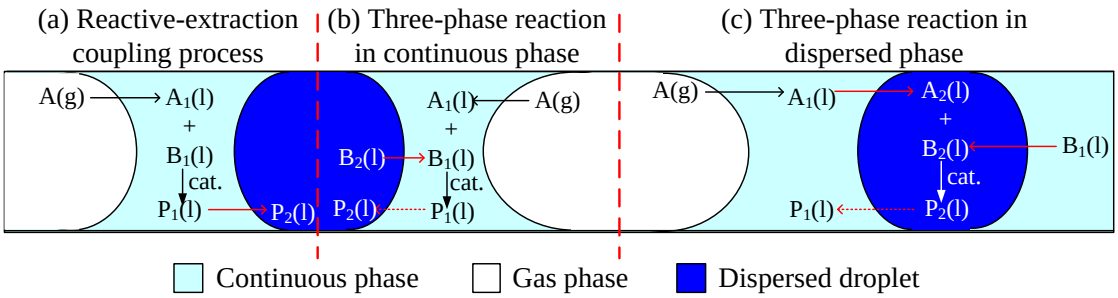

Figure 1. Schematics of mass transfer in a gas-liquid-liquid three-phase system in the microreactor. A, B are the reactants and P the product. The subscripts 1 and 2 represent the continuous phase and the dispersed phase, respectively. Catalyst and reaction both reside in either of the continuous phase and the dispersed droplet phase.

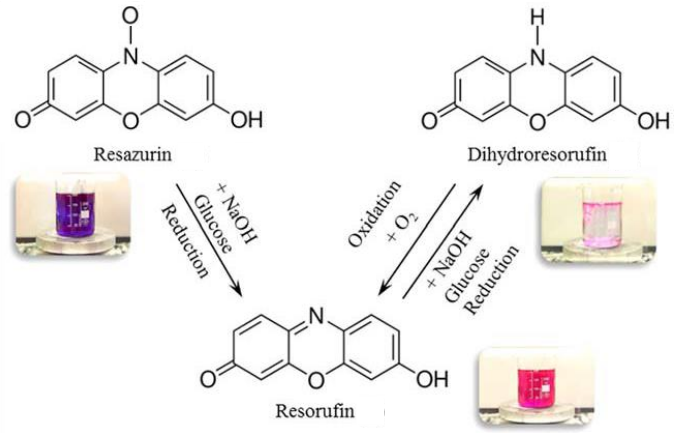

Figure 2. Reactions involved in the colorimetric method used for mass transfer characterization (reproduced from Ref[7]).

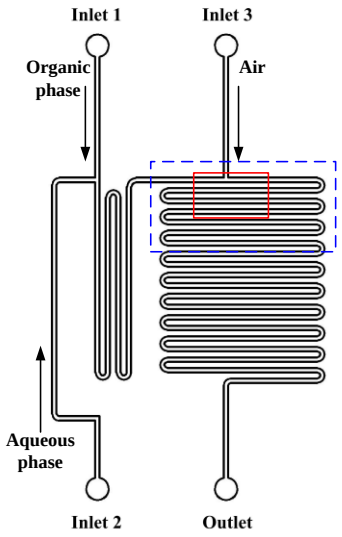

Figure 3. Structure of the microreactor (horizontally placed) used in three-phase flow and mass transfer study. The viewing sections for flow visualization and mass transfer characterization are indicated by the blue dotted box and the red solid box, respectively.

(a)

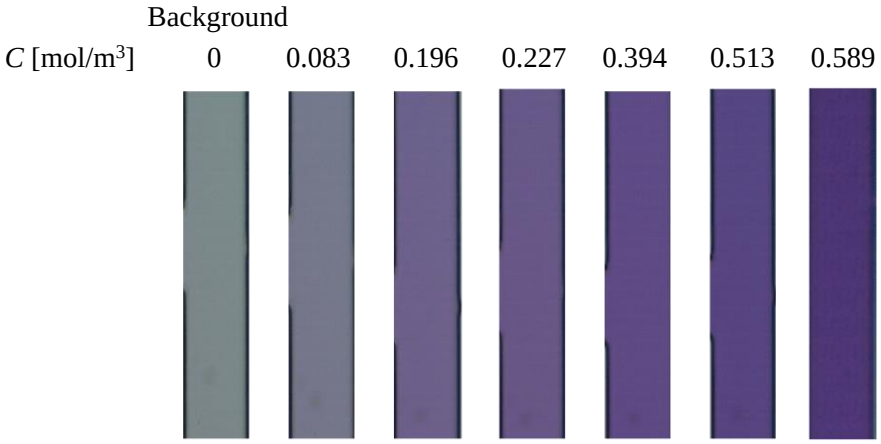

(b)

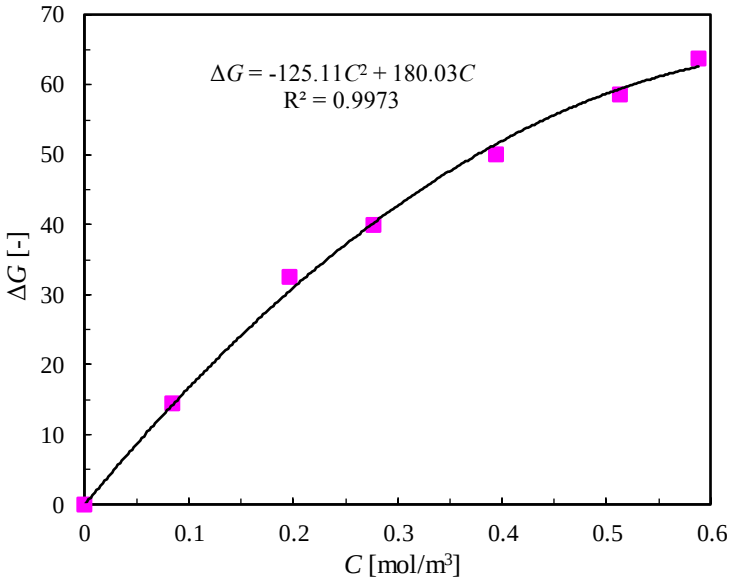

Figure 4. (a). Background and calibration images for the aqueous phase under various resazurin concentrations near the microreactor outlet; (b). Calibration curve between the equivalent oxygen concentration and the gray difference.

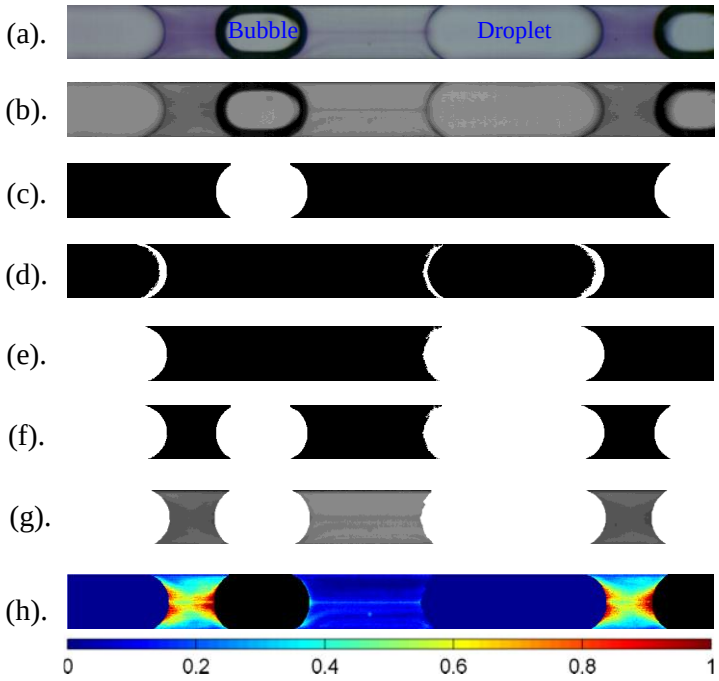

Figure 5. Identification process of bubbles and droplets in gas-aqueous-organic slug flow (G0.2-W0.6-O0.4, the gas, aqueous and organic phases are respectively air, 0.3 g/L resazurin solution with 20 g/L glucose and 20 g/L sodium hydroxide, and *n*-octane) in the microreactor: (a). original image; (b). gray image; (c) bubbles, (d) droplet caps, (e) droplets and (f) bubbles and droplets detected in binary images; (g) modified image after subtracting the background; (h) calibrated image with the normalized equivalent oxygen molar concentration (ranging from 0 to 1).

(a).

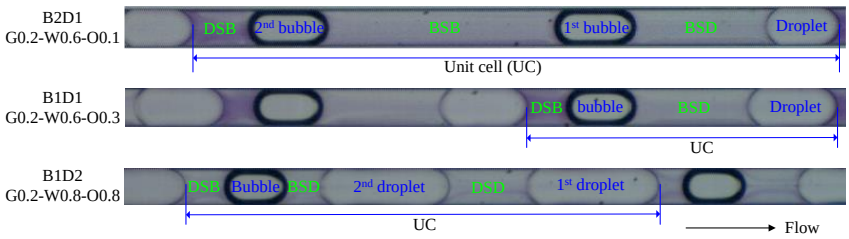

(b).

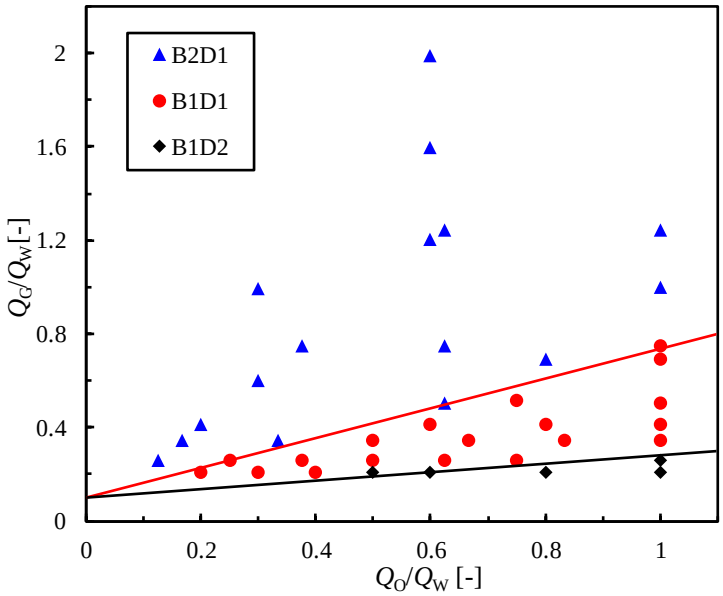

Figure 6. (a). Typical sub-regimes and slug types observed during experiments; (b). Sub-regime map of gas-liquid-liquid slug flow in the current microreactor.

(a).

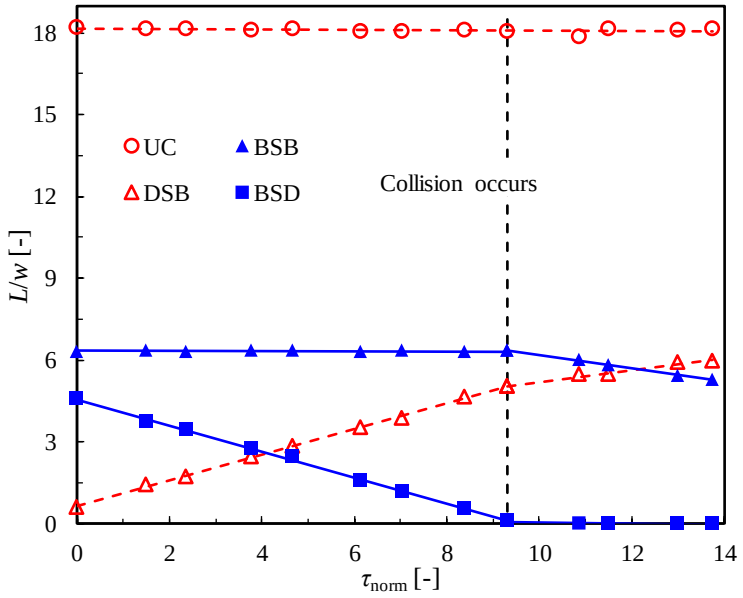

(b).

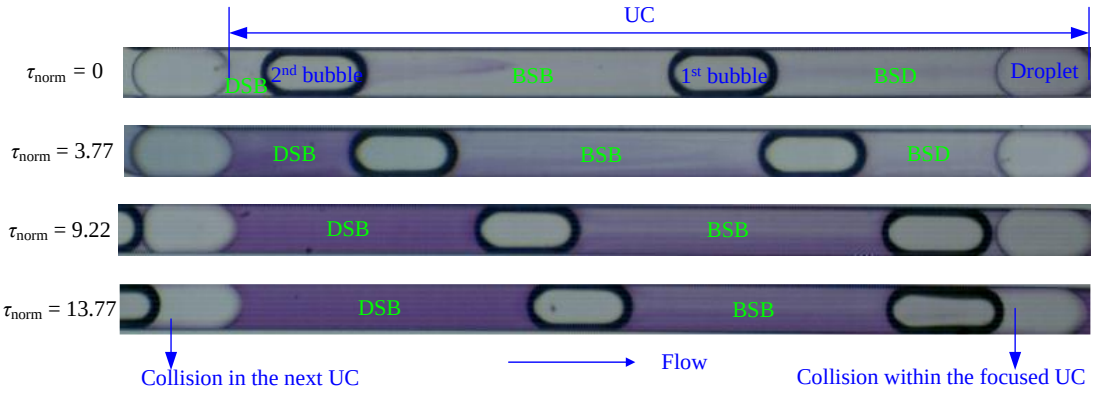

Figure 7. (a). Change of slug lengths with the dimensionless residence time and (b) the corresponding images within a unit cell under the sub-regime B2D1 in the microreactor. Operating condition: G0.2-W0.6-O0.1.

(a).

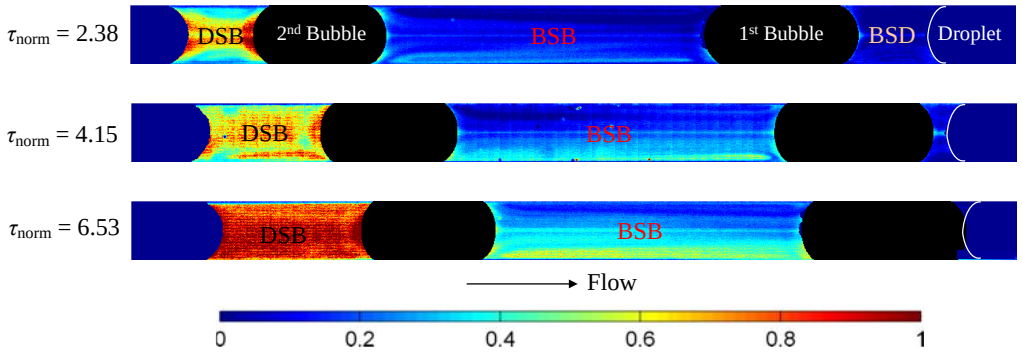
τ_{norm} = 2.38
DSB
2nd Bubble
BSB
1st Bubble
BSD
Droplet
τ_{norm} = 4.15
DSB
BSB
τ_{norm} = 6.53
DSB
BSB
Flow
0
0.2
0.4
0.6
0.8
1

(b).

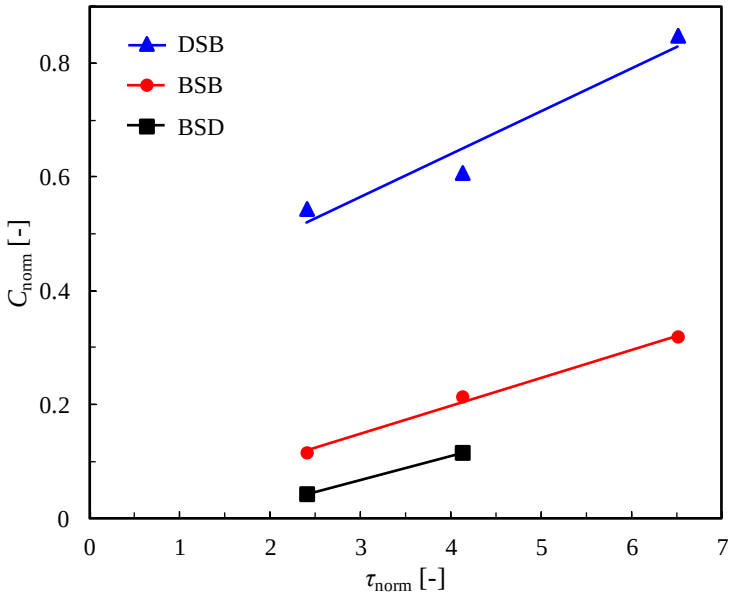
DSB
BSB
BSD
0.8
0.6
0.4
0.2
0
C_{nom} [-]
0
1
2
3
4
5
6
7
τ_{norm} [-]

(c).

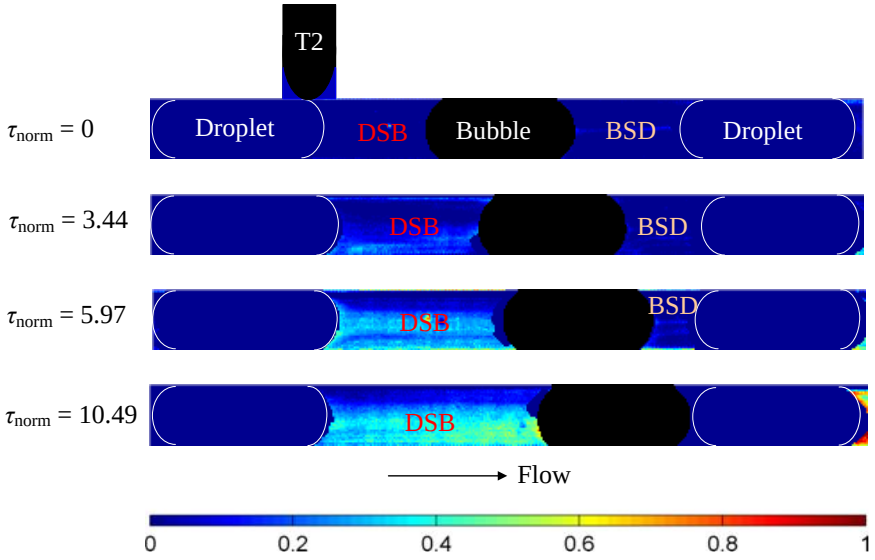

Figure 8. Normalized equivalent oxygen molar concentration (C_{norm}) in aqueous slugs under gas-liquid-liquid flow in the microreactor. (a) C_{norm} distribution and (b) the development of C_{norm} with the dimensionless residence time τ_{norm} along the microchannel under the sub-regime B2D1; operating condition: G0.2-W0.6-O0.1; (c) C_{norm} distribution within slugs DSB and BSD that have equal initial lengths under the sub-regime B1D1 at different τ_{norm} values; operating condition: G0.2-W0.6-O0.2.

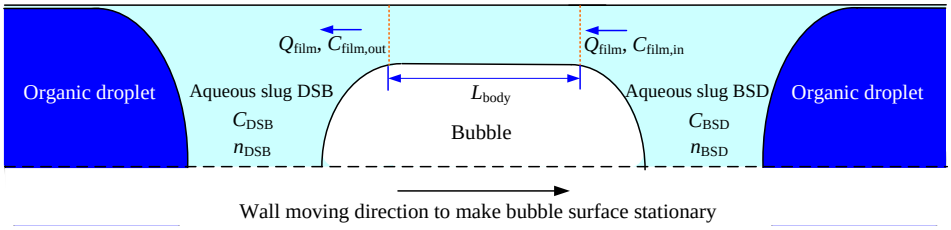

Figure 9. Sketch of mass transfer in the liquid film within a unit cell under the sub-regime B1D1, depicted in a half channel (microchannel corner being exaggerated).

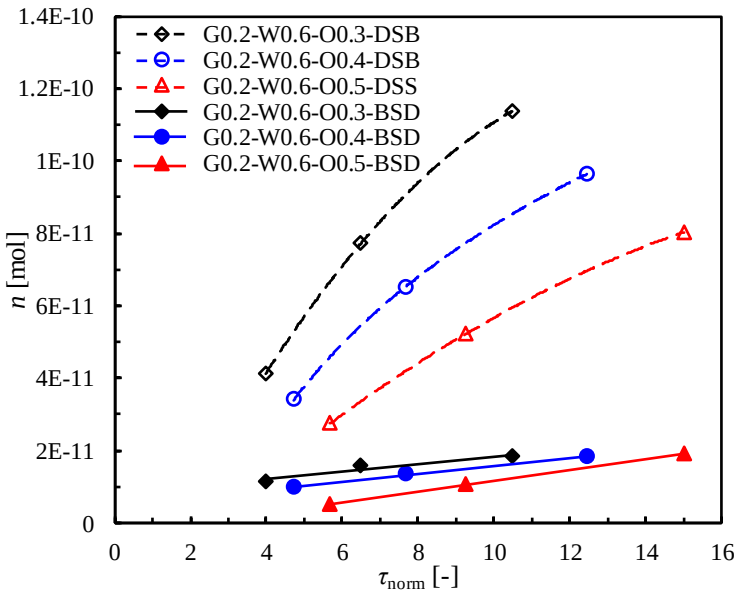

Figure 10. Accumulation of the amount of the equivalent oxygen in slugs BSD and DSB under the sub-regime B1D1 with operating conditions shown in the figure.

(a).

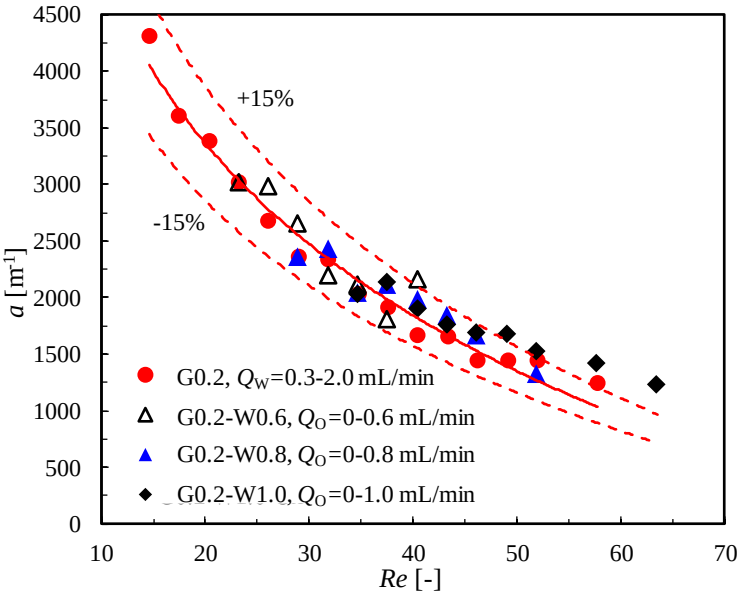

(b).

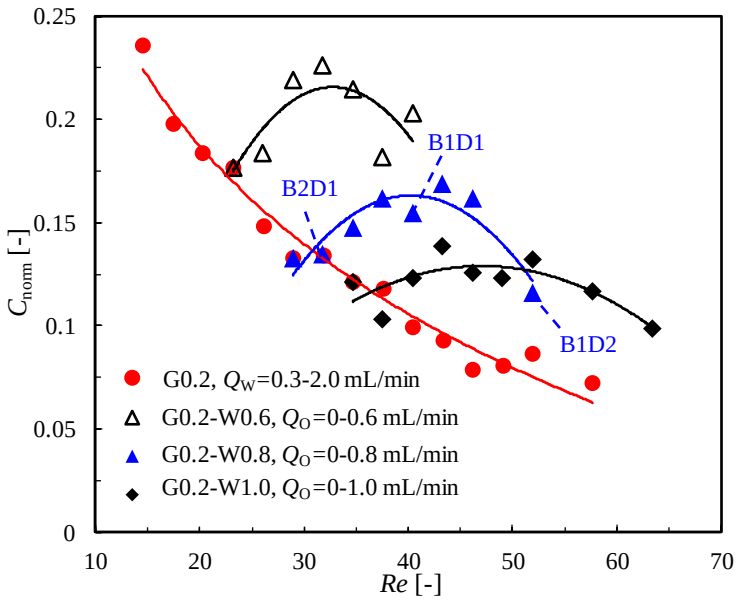

Figure 11. Effect of *Re* on (a) the specific interfacial area of bubbles and (b) the equivalent oxygen concentration under gas-aqueous and gas-aqueous-organic slug flows in the microreactor at a location of L_{ch} = 27 mm. In these figures, *Re* is directly related to the total liquid flow rate (i.e., Q_W+Q_O in three-phase system and Q_W in two-phase system).

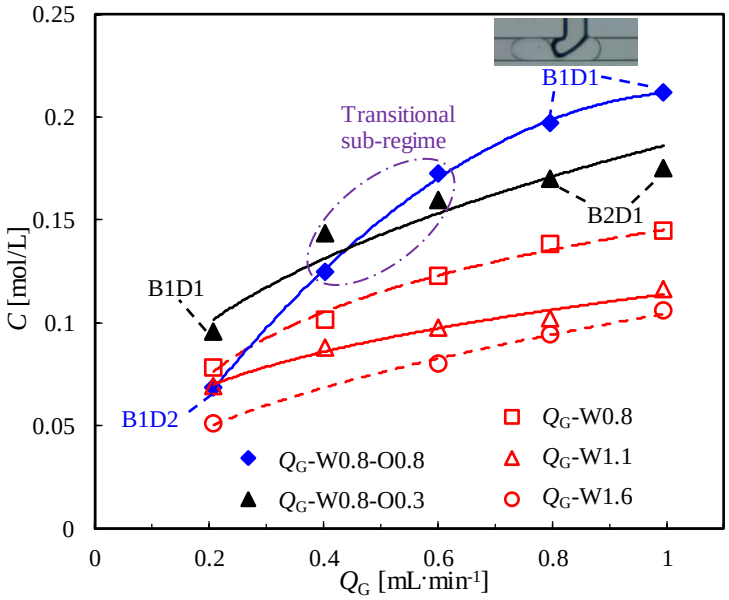

Figure 12. Effect of the gas flow rate on the mass transfer performance in both gas-aqueous (open marks) and gas-aqueous-organic (solid marks) slug flow at the fixed location of L_{ch}=27 mm. The sub-regimes are indicated in the figure as well.

Supplementary material

Hydrodynamics and local mass transfer characterization under gas-liquid-liquid slug flow in a rectangular microchannel

Yanyan Liu[1-3], Jun Yue[2], Chao Xu[1], Shuainan Zhao[1], Chaoqun Yao[1*] and Guangwen Chen[1*]

1. Dalian National Laboratory for Clean Energy, Dalian Institute of Chemical Physics, Chinese Academy of Sciences, Dalian 116023, China

2. Department of Chemical Engineering, Engineering and Technology Institute Groningen, University of Groningen, 9747 AG Groningen, The Netherlands

3. University of Chinese Academy of Sciences, Beijing 100049, China

1. Experimental Uncertainties with Image Processing

A typical image (magnification being ×2.0) of the calibration solution (resazurin concentration being 0.305 g/L) within the microchannel was shown in Fig. S1a, where the gray difference along the image length direction was abstracted. Fig. S1b shows that the gray difference in different channels (averaged from 100 images) somewhat varied along the image length direction (1280 pixels). In order to minimize the uncertainty with image processing, only the middle part of the image (pixels ranging from 280 to 1080) was analyzed for mass transfer study, rendering the experimental error below around 6%. An overall error for mass transfer study in a gas-aqueous system was further estimated to be within 10% (vide infra).

(a)

* Corresponding author. Tel.: +86-411-8437-9031, Fax.: +86-411-8469-1570

E-mail address: gwchen@dicp.ac.cn (G.W. Chen), superyao@dicp.ac.cn (C.Q. Yao)

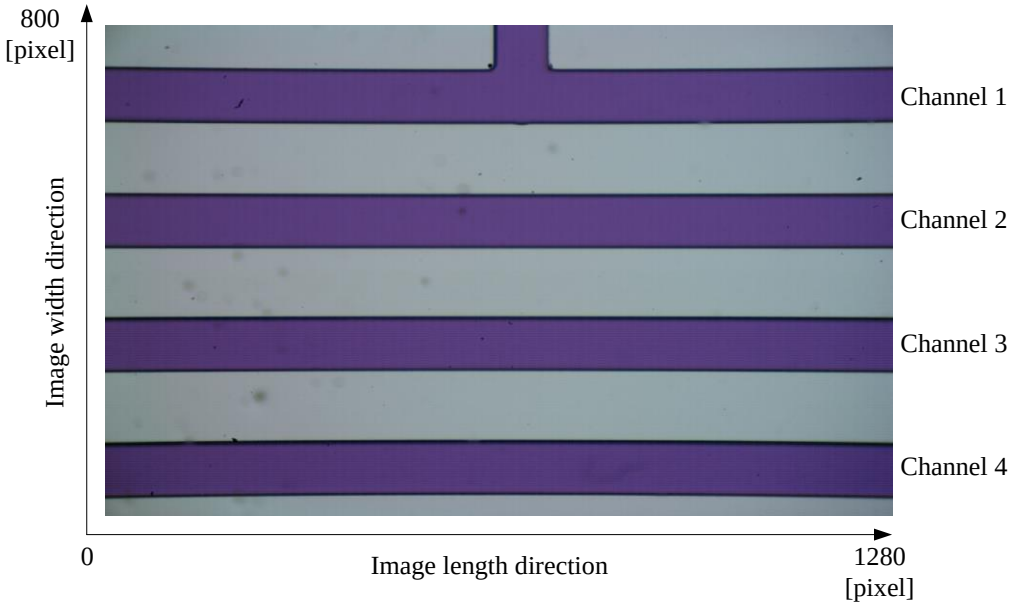

(b)

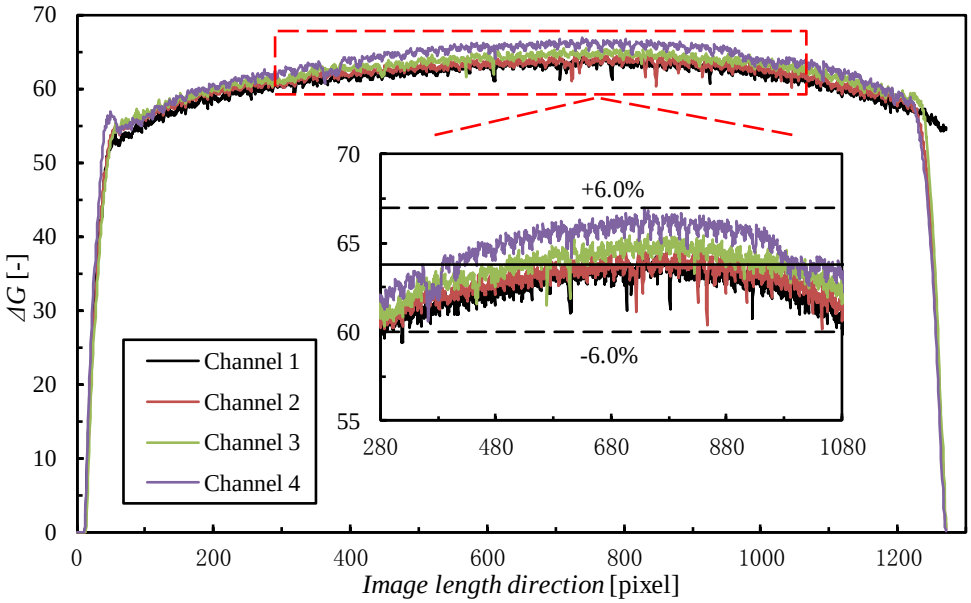

Figure S1. (a) An original image taken from the microchannel with a magnification of 2.0 (shooting area shown in Fig. 3) (b) Gray difference along the image length direction among channels. Operating conditions: resazurin concentration being 0.305 g/L or the equivalent oxygen molar concentration C=0.589 mol/L.

2. Method Validation

Before its use for gas-liquid-liquid slug flow, the colorimetric method was first validated

for mass transfer in gas-liquid slug flow in the current microreactor system. The equivalent oxygen concentration (C) in 30 aqueous slugs visualized at a downstream distance of 27 mm from T2 under the operating condition 'G1.0-W1.6' was measured (Fig. S2). It is seen that the concentration deviation was within 10%, indicating that the flow and mass transfer in the experiments were stable and the above image processing method is reliable. Given that oxygen (in air) was in much large excess to resazurin (in the aqueous phase) and that the oxidization of dihydroresorufin is a fast reaction, the oxygen concentration in the aqueous phase was fixed at its physical solubility ($C^* = 2.55\times10^{-4}$ mol/L based on the literature[1]) at the interface, and 0 in the liquid bulk[2]. According to the mass balance along the microchannel, one can finally get

$$U_W C = k_L a L_{ch} C^* \tag{S1}$$

where U_W is the superficial velocity of the aqueous phase ($=Q_W/(wh)$) and L_{ch} the distance between the concentration measurement location and T2. The overall volumetric mass transfer coefficient (k_La) represents the product of the liquid-side mass transfer coefficient (k_L) and the interfacial area (a), and is derived accordingly as

$$k_L a = \frac{U_W C}{L_{ch} C^*} \tag{S2}$$

Fig. S3 shows that k_La values under various operating conditions in the current microreactor system generally increased with both the superficial gas velocity (U_G) and aqueous velocity (U_W), and are ca. on the order of 1 s^{-1}. k_L according to Eq. (S3) was found to be on the order of ca. 10^{-4} m/s (figure not shown for brevity). These results are consistent with the literature results[3-5]. In conclusion, this colorimetric technique, including the imaging processing for the concentration measurement, is valid in the current system under the prevailing conditions.

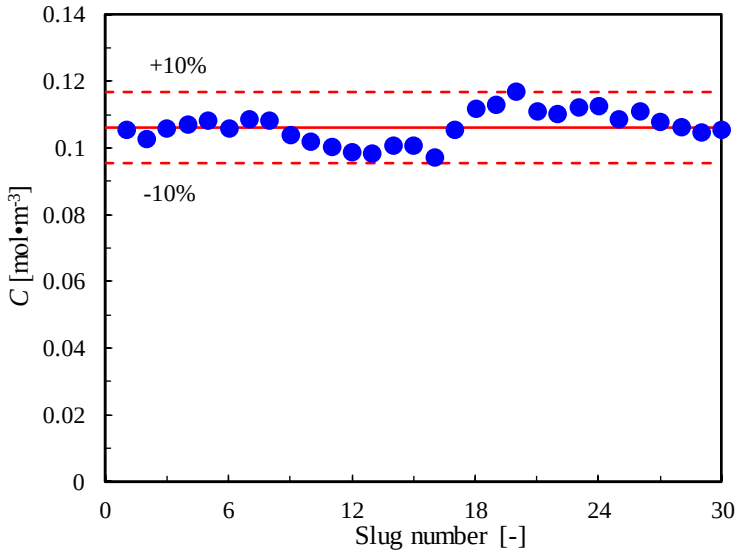

Figure S2. Equivalent oxygen concentration (*C*) in 30 aqueous slugs under the operating condition 'G1.0-W1.6' during gas-aqueous slug flow in the microreactor. The slugs were visualized at a downstream location of 27 mm after T2.

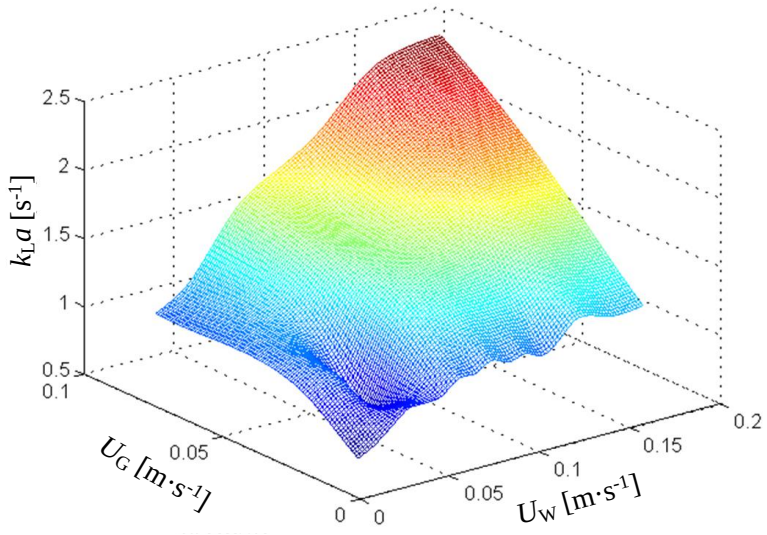

Figure S3. Relationship between the liquid-side volumetric mass transfer coefficient and the phasic superficial velocity at the downstream location of 27 mm after T2.

3. Definition of Dimensionless Numbers

1) Dimensionless oxygen concentration C_{norm}

$$C_{norm} = C/C_{max} \quad \text{(S3)}$$

where C is the equivalent oxygen concentration extracted from images, C_{max} (= 0.589 mol/m^3) is the maximum value determined by the applied resazurin concentration in the aqueous phase.

2) Dimensionless residence time τ_{norm}

τ_{norm} is defined as the ratio of residence time τ to the time interval that the slug flow needs to pass the length of a unit cell, therefore

$$\tau_{norm} = \tau / (L_{UC}/U_{tot}) \quad \text{(S4)}$$

where L_{UC} is the length of the rectangular microchannel, U_{tot} (=(Q_W+Q_O+Q_G)/wh) is the total superficial velocity of fluids in the microchannel. Note that Q_O = 0 for gas-aqueous two-phase system.

3) Reynolds number (Re) for the aqueous phase

$$Re = d_C U_{tot} \rho_{aq} / \mu_{aq} \quad \text{(S5)}$$

where d_C (= 2wh/(w+h) = 0.4 mm) is the hydraulic inner diameter of the rectangular microchannel used in this work, while ρ_{aq} and μ_{aq} are the density and viscosity of the aqueous phase, respectively.

4. Estimation of Mass Transfer Parameters

Figure S4 shows the cross-sectional shape of the dispersed bubble/droplet in a rectangular microchannel, where the corresponding parameters were calculated by Eqs. (S6-8) according to Musterd et al[6]. For bubbles in our case, the surface area of bubble body A_{body} (=A_{film}, the contact area between the film flow and bubble body) and bubble cap A_{cap} were respectively derived as Eqs. (S9-10). Therefore, the specific interfacial area of bubble(s) in a unit cell was estimated by Eq. (S11), where the length of unit cell L_{UC} was extracted from the recorded images.

$$r_t = \frac{h + w - \sqrt{h^2 + (\pi - 2)hw + w^2}}{4 - \pi} \tag{S6}$$

$$r_1 = \frac{h}{2} \tag{S7}$$

$$r_2 = \frac{h}{2} - r_t \tag{S8}$$

$$A_{body} = A_{film} = 2L_{body}(h + w + \pi r_t - 4r_t) \tag{S9}$$

$$A_{cap} = \pi r_1(w - 2r_t) + \pi r_2^2 + \pi^2 r_t(\frac{r_t}{2} + r_2) \tag{S10}$$

$$a = \sum A / (L_{UC} wh) \tag{S11}$$

The film volume V_{film} were approximated by

$$V_{film} = 2L_{body}\left[\delta_1(w - 2r_t + 2r_2) + \left(2 - \frac{\pi}{2}\right)r_t^2\right] \tag{S12}$$

where δ_1 was estimated by the correlation proposed by Aussillous and Quere[7], with an assumption of in a circular channel with a hydraulic inner diameter d_C (= $2wh/(w+h)$ = 0.4 mm). Then, the averaged film thickness δ in the rectangular microchannel is estimated by

$$\delta = \frac{V_{film}}{A_{film}} \tag{S13}$$

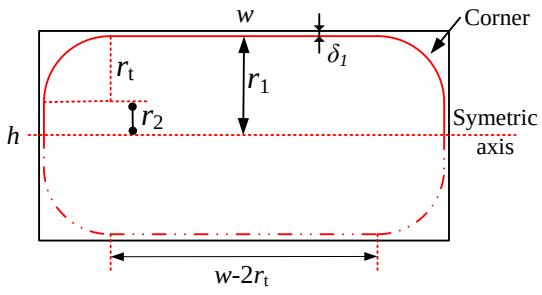

Figure S4. Cross sectional shape of a bubble or droplet in a rectangular microchannel and the corresponding geometrical parameters according to Musterd et al[6].

Therefore, the contact time between the bubble and the liquid film $t_{c,film}$ (= V_{film}/Q_{film}) is

obtained and used to calculate the Fourier number *Fo* (=$Dt_{c,film}/\delta^2$, where *D* is the diffusivity of oxygen in the aqueous phase), which is adopted to estimate the mass transfer coefficient in the film region[8]

$$k_{L,film} = 3.14\frac{D}{\delta} \quad (\text{for } Fo > 1.0) \tag{S14}$$

or

$$k_{L,film} = 2\sqrt{\frac{D}{\pi t_{C,film}}}\frac{\ln(1/\Delta)}{(1-\Delta)} \quad (\text{for } Fo < 0.1) \tag{S15}$$

where $\Delta = 0.7857\exp(-5.212Fo) + 0.1001\exp(-39.21Fo) + 0.0360\exp(-105.6Fo)...$

The liquid-side mass transfer coefficient in the cap area is calculated by[8]

$$k_{L,cap} = \frac{4}{\pi}\sqrt{\frac{D(2U_{tot} - U_B)}{d_c}} \tag{S16}$$

where U_B is the bubble velocity that was measured directly from the recorded images.

5. Phase Dispersion Under the Sub-regime B1D1

Fig. S5 shows the size laws of dispersions (bubbles, organic droplets and aqueous slugs) during gas-liquid-liquid slug flow under the sub-regime B1D1 in the current microreactor, where the initial length of the slug DSB equals 0 and the initial length of the slug BSD is denoted as $L_{BSD,0}$. The size laws for the droplet and the initial aqueous slug BSD are respectively expressed as $L_{bubble}/w = 1.88Q_O/Q_W + 1.48$ and $L_{BSD,0}/w = 1.05Q_W/Q_O + 1.36$, which agrees with that in two-phase system. This concordance is reasonable since the aqueous-organic two-phase flow was first formed at the first T-junction (T1), and the addition of gas phase in the second T-junction (T2) did not squeeze the original aqueous slug off (i.e., initial length of aqueous slug DSB $L_{DSB,0} = 0$). However, the length of bubbles (which was generated at T2) was found to be related to both Q_G/Q_W and Q_G/Q_O by the correlation

$L_{bubble}/w = 3.06Q_G/Q_W + 1.52Q_G/Q_O$. The different coefficients associated with the terms Q_G/Q_W and Q_G/Q_O indicate that the two terms contributed differently on the length of bubbles generated. This is because that the bubble was subsequently cut/sheared off by organic droplet and aqueous slug, of which interfacial tensions with gas are different. Therefore, distinct coefficients were derived. All the experimental results were in a range of ±15% of the predictions, as shown in Fig. 5S.

(a)

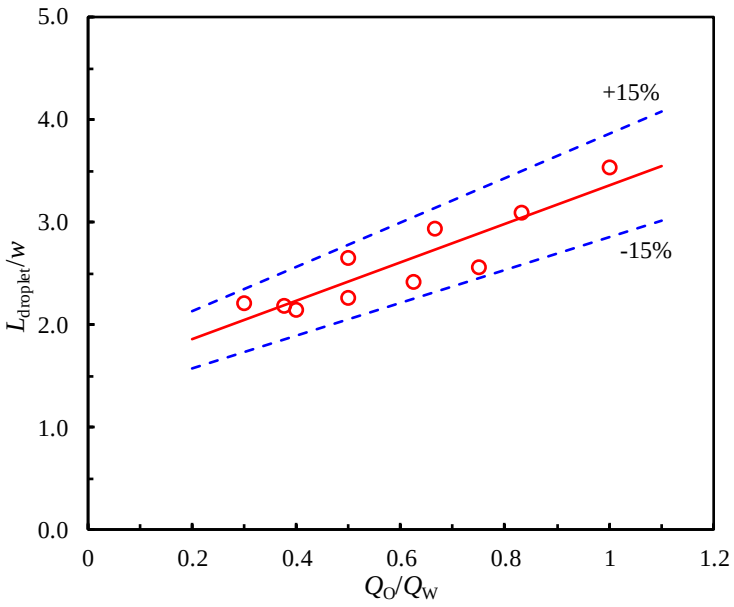

(b)

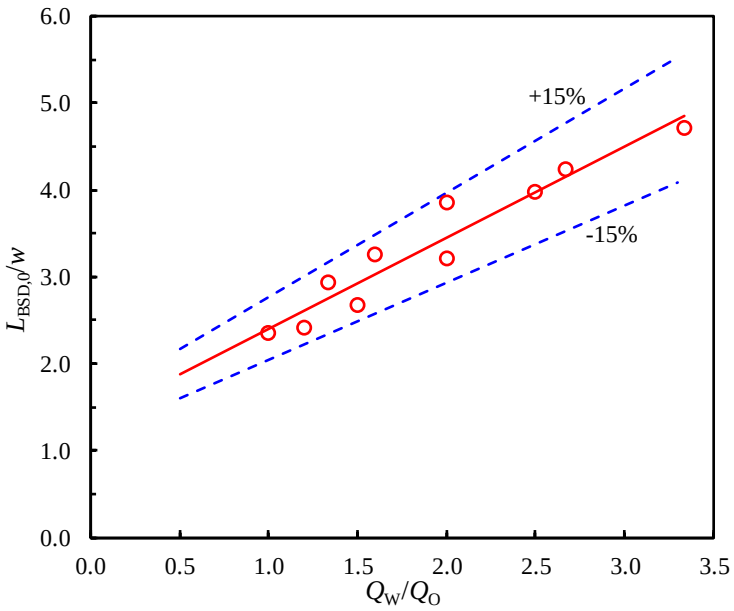

(c)

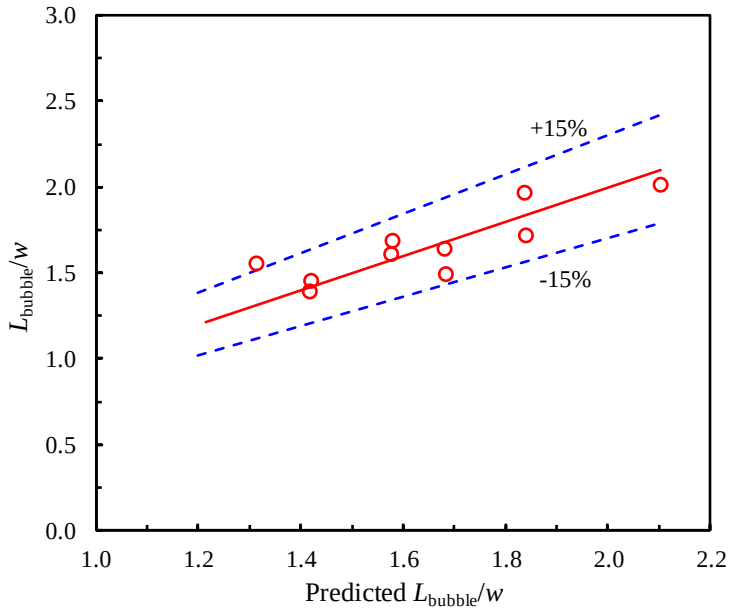

Figure S5. Size laws of (a) the organic droplets, (b) the aqueous slug BSD formed right after T2and (c) bubbles in gas-liquid-liquid slug flow under the sub-regime B1D1 (fixed gas flow rates at 0.2 mL/min while aqueous and organic flow rates were changing) in the current microreactor.

References

1. Yang LX, Dietrich N, Hébrard G, Loubière K, Gourdon C. Optical methods to investigate the enhancement factor of an oxygen-sensitive colorimetric reaction using microreactors. AIChE J. 2017;63(6):2272-2284
2. Dietrich N, Loubière K, Jimenez M, Hébrard G, Gourdon C. A new direct technique for visualizing and measuring gas-liquid mass transfer around bubbles moving in a straight millimetric square channel. *Chem. Eng. Sci.* 2013;100:172-182.
3. Yao CQ, Dong ZY, Zhao YC, Chen GW. An online method to measure mass transfer of slug flow in a microchannel. *Chem. Eng. Sci.* 2014;112:15-24.

4. Yue J, Chen GW, Yuan Q, Luo LA, Gonthier Y. Hydrodynamics and mass transfer characteristics in gas-liquid flow through a rectangular microchannel. *Chem. Eng. Sci.* 2007;62(7):2096-2108.
5. Yang LX, Dietrich N, Loubière K, Gourdon C, Hébrard G. Visualization and characterization of gas-liquid mass transfer around a Taylor bubble right after the formation stage in microreactors. *Chem. Eng. Sci.* 2016;143:364-368.
6. Musterd M, van Steijn V, Kleijn CR, Kreutzer MT. Calculating the volume of elongated bubbles and droplets in microchannels from a top view image. *RSC Adv.* 2015;5(21):16042-16049.
7. Aussillous P, Quéré D. Quick deposition of a fluid on the wall of a tube. *Phys. Fluids.* 2000;12(10):2367.
8. Donaldson AA, Macchi A, Kirpalani DM. Predicting inter-phase mass transfer for idealized Taylor flow: A comparison of numerical frameworks. *Chemical Engineering Science.* 2011;66(14):3339-3349.